JOURNAL OF CATALYSIS 80, 172–187 (1983)

Study of Fischer–Tropsch Synthesis over Fe/SiO_2: Reactive Scavenging with Pyridine and Cyclohexene

CHIAZUAN JEFF WANG AND JOHN G. EKERDT[1]

Department of Chemical Engineering, University of Texas, Austin, Texas 78712

Received April 22, 1982; revised October 19, 1982

The synthesis of hydrocarbons from H_2 and CO was studied on a silica-supported Fe catalyst. The synthesis was carried out at 1.54 atm and 200 to 255°C in a differential reactor. Conversion of CO never exceeded 2%. The working catalyst is achieved by transforming Fe_2O_3 into a mixture of Fe_3O_4, bulk carbides, and iron under synthesis conditions. Synthesis product distributions and the rate of methane formation are reported. Trends in CO_2 formation and the presence of cyclic hydrocarbons, saturated and unsaturated, suggest the presence of some Fe_3O_4 at the catalyst surface. Cyclohexene addition to the feed generates low concentrations of alkyl-substituted cyclohexenes and cyclohexanes consistent with reported scavenging studies over Ru. Pyridine addition to the feed generates alkyl-substituted pyridines. The results suggest that the scavengers react with species involved in chain propagation.

INTRODUCTION

Fischer–Tropsch synthesis of hydrocarbons over a wide range of molecular weights and varying composition is possible over iron-based catalysts, making them attractive commercial catalysts. An understanding of the reaction pathways to the various products and the catalytic forces which control these reactions is needed to improve and control selectivity. Numerous experimental techniques have been applied in recent investigations of the catalytic phenomena including: XPS (*1, 2, 14*), Auger (*2, 3*), Mössbauer (*4–10*), XRD (*4, 7, 8, 10, 14*), ir (*11*), and rate measurements (*1–6, 8–10, 12–14*).

Investigations of Fe-based catalysts have shown that the chemical composition of the iron phase generally changes during the Fischer–Tropsch reaction (*1–10, 14, 15*). These investigations include foil, single crystal, and dispersed iron systems. Iron is seen to form a mixture of bulk carbides and an inactive carbon overlayer depending upon the temperature, H_2/CO ratio, extent of CO conversion, and the duration of the reaction. The various forms are the result of the complex oxidation–reduction reactions among Fe_3O_4, Fe, and the carbides. It has also been suggested that the surface composition changes with synthesis conditions (*10, 12, 14*) and that the surface and bulk may exist as different iron phases.

Madon and Taylor (*12*) and Satterfield and Huff (*13*) in recent rate studies have shown that iron-based synthesis products satisfy the distribution commonly referred to as a Schultz–Flory distribution. Anderson's review of the Schwartzheide tests contains similar plots (*16*). Satterfield and Huff (*13*) obtained a linear relation between the log of the mole fraction of product C_n and the carbon number, n, extending between 1 and 20 by including oxygenated products. Schultz–Flory plots are an indication that the synthesis proceeds by a stepwise process. Madon and Taylor (*12*) and Anderson (*16*) observe a bend in the distribution plots at carbon numbers of 22 and 9–12, respectively. Madon and Taylor propose that the bend is due to chain growth taking place on different types of sites, each with different chain growth probabilities.

The chain propagation step occurring

[1] To whom all correspondence should be addressed.

0021-9517/83/030172-16$03.00/0

during Fischer–Tropsch synthesis has been discussed in recent reviews (*17, 18*). While it remains to be proven conclusively, a scheme involving methylene insertion into a growing alkyl chain appears most likely in light of the recent work of Brady and Pettit (*19, 20*). This mechanism is proposed to describe chain growth over a variety of metals, including iron and ruthenium.

The purpose of this paper is to report the application of reactive scavengers over iron as a means to study the propagation reaction. The technique has been shown to remove hydrocarbon fragments of varying length from a ruthenium surface (*18, 21, 22*). The technique involves injecting a probe molecule into the reacting mixture and alkylating it with hydrocarbon fragments present on the catalyst surface. Fragments of varying carbon number alkylate the probe to give a distribution of substituted-probe molecules. The alkylated-probe distribution is dependent upon the synthesis conditions. Results over ruthenium are interpreted to support the presence of methylene (*18*) and alkyl fragments on the surface (*18, 21*). Scavenging provides an indirect means to measure the effect of the synthesis conditions on the surface species participating in the propagation reaction.

The successful application of pyridine and the complications inherent with cyclohexene as scavengers will be discussed in this paper. The influence of the synthesis variables upon scavenged product distributions and the implications concerning the reaction mechanism will be discussed in a future paper.

EXPERIMENTAL

Apparatus

The apparatus, shown schematically in Fig. 1, consists of three sections: a gas handling section, a reactor, and a product collection and analysis section. The reactant gases are metered and blended to the desired composition and flow rate by monitoring the pressure drop through capillary tubing. Multiport ball valves are used to select the path the gas will take before venting through a gas chromatograph sample valve. Aside from the copper tubing and brass fit-

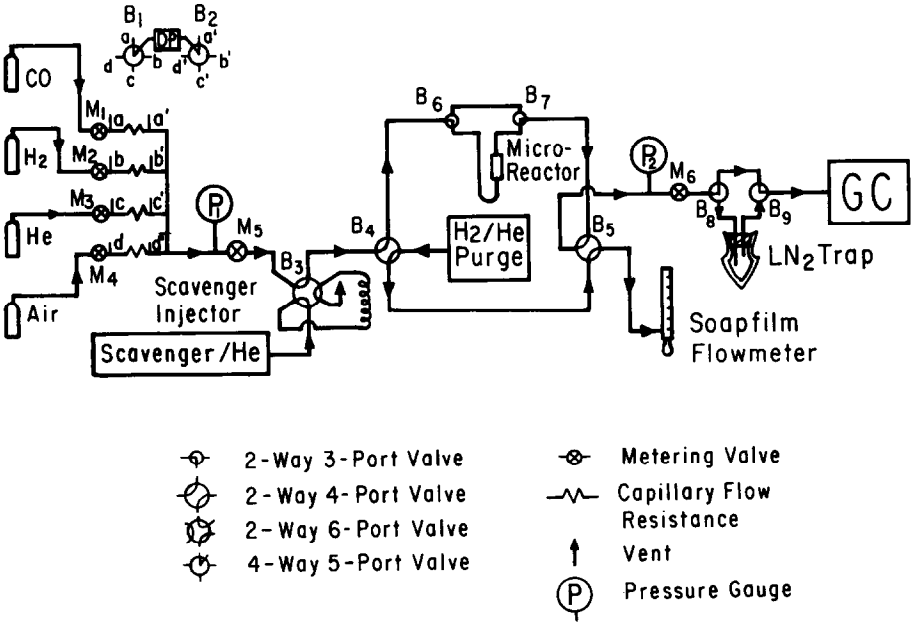

FIG. 1. System schematic.

tings used to connect and regulate carbon monoxide all tubing, fittings and valves are stainless steel. Reactor effluent gases are reduced to atmospheric pressure at valve M6. The tubing, valves, and fittings between the reactor, the trap, and the gas chromatograph are maintained at 80 to 100°C.

The reactor is a 2-in. section of 0.25-in.-o.d. stainless-steel tubing with 0.25- to 0.125-in. Swagelok unions on both ends. Catalyst is contained in the reactor tube by positioning quartz cloth in the union shoulders. The reactor and inlet gas lines are immersed in a constant temperature sand bath regulated to a precision of ±1°C.

Reaction and Scavenging Techniques

All work reported in this paper was carried out at 1.54 atm of total pressure (1 atm equals 101.3 kPa) and temperatures ranging from 220 to 255°C. The H_2/CO ratio ranged between 1 and 9. The total volumetric flow rate was varied between 100–240 SCCM.

The catalyst powder was pressed into wafers approximately 0.003 in. thick and crumbled before placing in the reactor. Less than 0.5 g of catalyst was charged to the reactor. The WHSV (volumetric gas flow rate at inlet conditions in $cm^3/hr/g$ of catalyst) ranged between 15,840 and 46,780. The actual value is indicated, where appropriate, within the text. Carbon monoxide conversion never exceeded 2% at the feed rate and catalyst loading employed.

Iron oxide on silica, Fe_2O_3/SiO_2, was conditioned for 6 days by passing a $\frac{4}{1}$ H_2/CO mixture over the catalyst at 230°C. This was found sufficient to convert the Fe_2O_3 into a mixture of Fe_3O_4, carbides, and possibly α-Fe, which displayed a stable steady-state activity. A conditioned catalyst was always exposed to hydrogen and carbon monoxide between 200 and 250°C to maintain the active form. The catalyst was allowed to adjust to new synthesis conditions for at least 12 hr before data were collected.

A stream of helium was sparged through the scavenger, cyclohexene, or pyridine, at room temperature and vented through an 80-μl loop on a six-port sample valve. A pulse of the scavenger was added into the reactor feed gas by actuating the valve. The injection and collection protocol changed over the course of the work. Sixty to one-hundred twenty pulses of cyclohexene at 60-s intervals were injected and the reactor effluent was diverted to the liquid nitrogen trap for 25 s after each injection. Increasing the number of pulses increases the total amount of scavenged product collected. The number was varied in an attempt to generate detectable quantities of scavenged products. The reactor effluent was not trapped continuously to minimize dilution of the scavenged products with Fischer–Tropsch synthesis products. Pyridine was found to be much more efficient at scavenging fragments and three to ten injections over a 15-min interval were used. During the 15-minute interval all the reactor effluent was directed through the trap.

The trap is a 50-ml pear-shaped boiling flask. The collected samples were stored in the flask at −10°C for analysis at a later time. Samples were never stored for more than 48 hr.

Product Analysis

Most of the analysis was conducted using a Varian 3760 gas chromatograph fitted with two packed columns and one capillary column. Eighth-inch-outside diameter stainless-steel columns of Chromosorb 106 (12-ft length) and 20% OV-101 on Chromosorb P-AW (20-ft length) were used to analyze hydrocarbons below C_7. The capillary column, used for C_7 and above hydrocarbons, was a Quadrex fused silica column 50 × 0.235-mm i.d., coated with OV-101.

Chromosorb 106 was used to separate reactants, H_2 and CO, from light products, CO_2, CH_4, C_2H_4, C_2H_6, C_3H_6, and C_3H_8. This column was connected to a thermal conductivity detector. The OV-101 packed column was used to separate C_4 through C_6 hydrocarbons and was connected to a flame

ionization detector. The capillary column was connected to a similar detector. Each column required a different temperature schedule for maximum component resolution, therefore, only one column was operated at a time.

One cubic centimeter of gas was injected into the packed columns using a heated (80–100°C) six-port sample valve. The packed columns were calibrated each day using two Matheson Certified Standard gas mixtures containing CO, CO_2, CH_4, C_2 to C_5 *n*-alkanes and primary *n*-olefins, and hexane at different concentrations. Product gas concentrations were determined by comparing the product's peak height to the peak heights for the standards.

The trapped products were analyzed using the capillary column in the Varian GC or in a Finnegan 4023 GC–MS. The products were washed from the sides of the flask and extracted from any water with 0.05 ml of diethyl ether. A splitless Grob-type injector was used on both instruments and 1.0 to 2.0 μl was injected.

Elution characteristics for the column were established using the GC–MS. Component assignment was performed by a computer library search of the five major fracturing peaks remaining after standard enhancement. The computer is forced to make an assignment and provides three quantities which represent the confidence of the assignment, fit, refit, and purity. Fit values greater than 900, boiling points expected for the unknown component's retention times, examination of the mass fracturing pattern, and when possible injection of pure components were used to assign the identity to an eluted component. The capillary column was operated under identical temperature cycles on the Varian GC to maintain the same component elution order. Standard mixtures were injected to fix the position of known compounds on a chromatogram. Identification of peaks eluting from the GC were made by comparing the chromatograms for the two instruments.

Catalyst Preparation and Characterization

The supported iron catalyst was prepared by the incipient wettness technique using 2.0 ml of solution, $Fe(NO_3)_3 \cdot 9H_2O$ in distilled water, per gram of silica, Cab-O-Sil HS-5. The impregnated support was vacuum-dried in a rotary evaporator at 60°C for 42 hr and calcined with zero air (21% O_2, 79% N_2) at 300°C for 1 hr, followed by 20 hr at 400°C. The catalyst was cooled in the zero air and stored in a dessicator.

Metal content was determined by inductively coupled atomic emission spectroscopy. The catalyst was determined to be 20.44 wt% Fe_2O_3. Iron, iron oxides, and iron carbides were determined using a General Electric Model XJF-7 X-ray diffractometer. Cu$K\alpha$ radiation diffracting from a graphite monochrometer was used. Particle size was estimated using the line broadening technique.

Materials

Hydrogen (Matheson UHP, 99.999%) was passed through a Matheson deoxo cylinder to remove any oxygen. Carbon monoxide (Matheson UHP, 99.8%) was heated to 95°C over molecular sieves to decompose metal carbonyls.

Cyclohexene (Aldrich 99%) was purified by distillation over sodium. Pyridine (MCB spectral grade) was used without further purification.

RESULTS AND DISCUSSION

Catalyst Induction

It is well established that Fe or Fe_3O_4 will convert into one or more carbide phase under synthesis conditions (*1, 2, 4–10, 14–16, 23*). The rates at which the carbide phases convert and the changes in synthesis activity and synthesis selectivity are also reported. Uncertainty in iron phase composition can complicate analysis of data. In an attempt to minimize the uncertainty, the catalyst used in this study, 20.44 wt% Fe_2O_3/SiO_2, was conditioned under $\frac{4}{1}$

H_2/CO (P_{CO} = 0.22 atm) at 230°C for 6 days prior to use and was rarely exposed to temperatures in excess of 250°C.

Time-dependent methanation activity and low weight product selectivity are presented in Figs. 2 to 4. These figures display Fischer–Tropsch data over a 40-day period at a common temperature of 230°C and a WHSV of 15,840. The H_2/CO ratio and partial pressure of CO vary between 3.8 to 4.3 and 0.20 to 0.23 atm, respectively. Some of the scatter of the data may be due to the slight random variation in reactant partial pressures. After the sixth day this catalyst was also exposed to other pressures and temperatures.

Figure 2 demonstrates the effect the induction period has on methanation activity. After approximately 150 hr the activity reaches a steady value. Activity decreases slightly after 400 to 500 hr. Reymond *et al.* (*14*) report a time-dependent increase followed by a decrease in methanation activity for unsupported α-Fe_2O_3. Their study at 250°C and $\frac{9}{1}$ H_2/CO showed a maximum at 5.5 hr and no leveling off of the activity over a 20-hr period. The extended activity

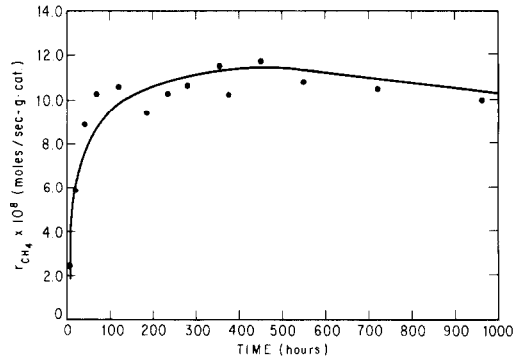

FIG. 2. Rate of methane formation as a function of time on stream (230°C, nominally $\frac{4}{1}$ H_2/CO, nominally 0.22 atm CO, 15,840 WHSV).

observed in this study may be due to the fact that the catalyst used in Figs. 2 to 4 never exceeded 250°C and that most experiments were performed at temperatures less than 240°C.

Figure 3 shows that the distribution to total C_2 to C_5 hydrocarbons (branched and normal alkanes and olefins) does not change appreciably during the induction period. Only the C_2s increase relative to methane during the first 150 hr. These results indicate that the selectivity to low weight

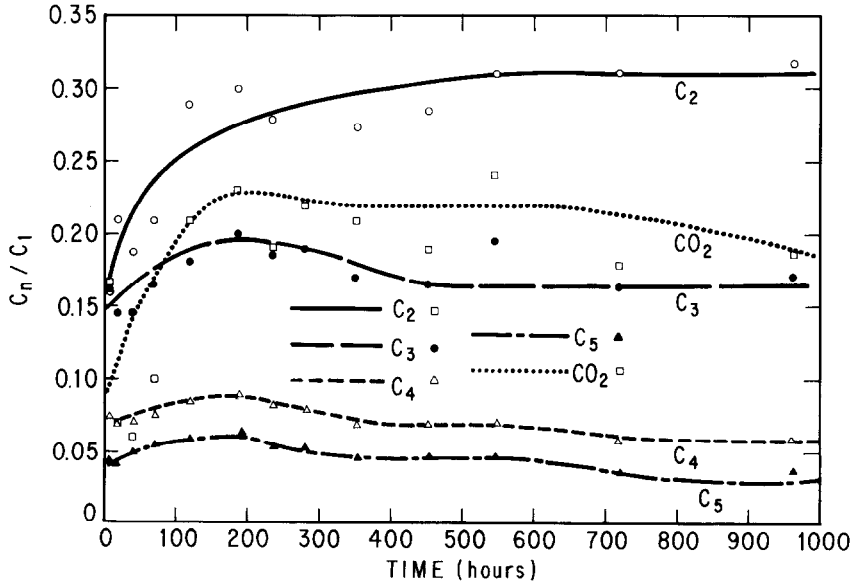

FIG. 3. Fischer–Tropsch synthesis selectivity to low weight hydrocarbons as a function of time on stream (230°C, nominally $\frac{4}{1}$ H_2/CO, nominally 0.22 atm CO, 15,840 WHSV).

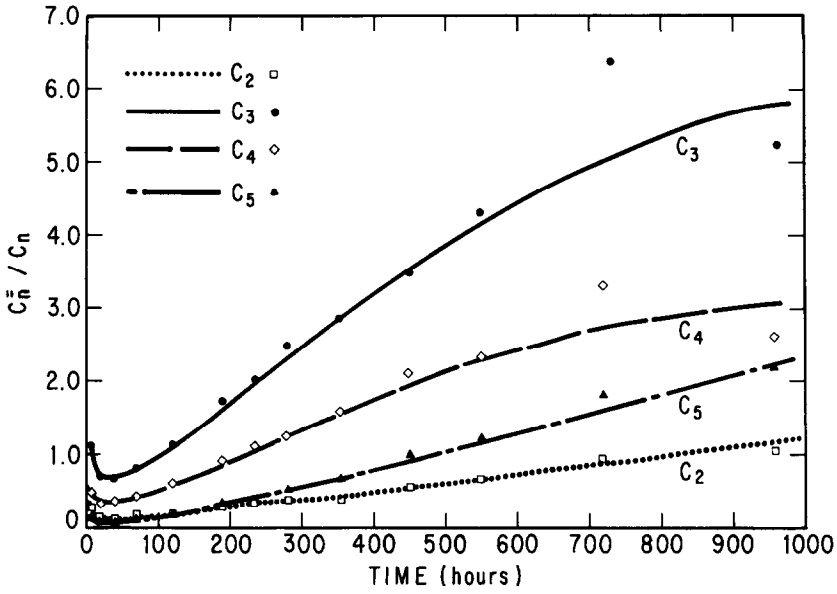

FIG. 4. Primary olefin to normal alkane selectivity as a function of time on stream (230°C, nominally $\frac{1}{1}$ H/CO, nominally 0.22 atm CO, 15,840 WHSV).

hydrocarbons is relatively independent of total activity. The C_1 to C_5 hydrocarbons increase in activity at approximately the same rate. The time-dependent distribution of C_6^+ hydrocarbons was not monitored. High weight products are synthesized during the early stages of induction. A liquid sample collected 4 hr after exposing Fe_2O_3 to H_2 and CO was found to contain hydrocarbons up to C_{12}, the upper limit investigated.

Carbon dioxide selectivity increases over the first 150 hr and is essentially constant for the remaining 850 hr. Carbon dioxide is probably formed in a secondary process via the water–gas shift reaction (*12*). Increasing shift activity suggests that the Fe_2O_3 is converting into Fe_3O_4 during the induction period.

Figure 4 presents the α-olefin to n-alkane ratio for small hydrocarbons. The ratios pass through a minimum, returning to their initial value after approximately 120 to 140 hr on stream, and continue to increase over the course of the time period studied. Ott *et al.* (*1*) report a similar trend for C_2 and C_3 over unsupported fully reduced iron at 300°C, but within a period of 400 to 500 min. The change was related to carburization of the iron.

The activity and product distribution trends shown in Figs. 2 to 4 suggest that the Fe_2O_3/SiO_2 is undergoing a rapid transformation into a different active phase during the first 150 hr. This is followed by a slow transformation over the remaining 700 hr. This slow change giving rise to the increasing olefinic nature of the product.

The conversion of unsupported Fe_2O_3 (*14*) into Fe_3O_4 and χ-carbide is reported at 250°C. Amelse *et al.* (*6*) convert 90% reduced Fe_2O_3 into carbides. Unmuth *et al.* (*24*) report that α-Fe_2O_3/SiO_2 reduces to Fe_3O_4 prior to reducing to Fe under H_2 at 425°C. In a separate study, Unmuth *et al.* (*8*) demonstrate that Fe/SiO_2 is converted to a mixture of carbides at $\frac{3}{1}$ H_2/CO and 256°C.

X-ray diffraction (XRD) was used to characterize the state of the catalyst. The results are presented in Fig. 5. Composition assignments are based upon published diffraction patterns (*25*). Table 1 lists the location of the primary peak for the various

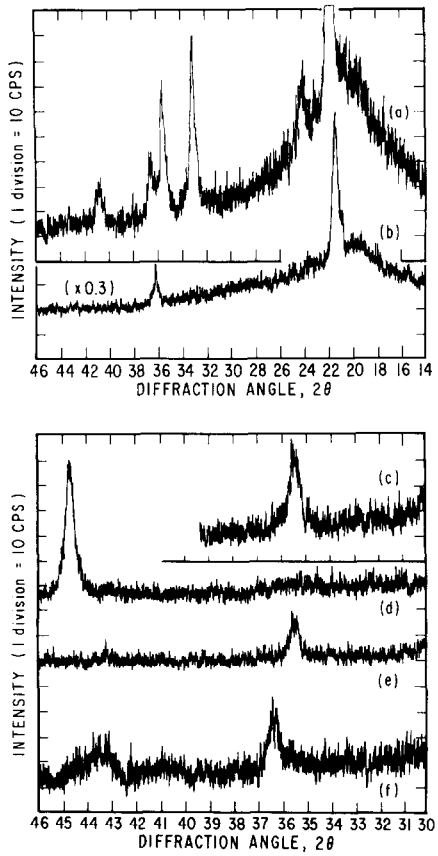

FIG. 5. X-Ray diffraction patterns. (a) 20 wt% Fe_2O_3/SiO_2 (covered with polyethylene film), (b) 25.4-μm-thick polyethylene film, (c) partially reduced 10 wt% Fe_2O_3/SiO_2, (d) fully reduced 20 wt% Fe_2O_3/SiO_2, (e) catalyst after 162 hr of reaction at $\frac{4}{1}$ H_2/CO and 230°C, and (f) catalyst after 56 days of use (covered with polyethylene film).

phases reported by other researchers.

Polyethylene was used to cover the fresh catalyst and the catalyst which had been exposed to hydrogen and carbon monoxide between 200 and 255°C for 56 days. The catalyst was transferred to a glass slide and covered with the 25.4-μm-thick polyethylene film in an invert environment to minimize oxidation. Amelse *et al.* (*6*) have shown that air oxidation is not rapid, therefore, all other XRD patterns were recorded in the absence of polyethylene.

The fresh catalyst diffraction pattern, pattern a, is identified as α-Fe_2O_3 with an average particle size of 240 Å. The single-phase patterns for Fe_3O_4, pattern c, and α-Fe, pattern d, were determined using two separate weight loadings. The Fe_3O_4 pattern was observed after reducing 10 wt% Fe_2O_3/SiO_2 at 400°C for 6 hr under H_2. Continued reduction of the Fe_3O_4 to α-Fe was realized by heating under H_2 for an additional 14 hr at 400°C and 1 hr at 430°C. The α-Fe pattern presented in Fig. 5 was obtained with 20.4 wt% Fe_2O_3/SiO_2 which was subjected to H_2 at 460°C for 24 hr to ensure complete reduction.

Catalyst was analyzed after exposing 20.44 wt% Fe_2O_3/SiO_2 for 162 hr to $\frac{4}{1}$ H_2/CO, 0.22 atm of CO at 230°C. The peak centered at 2θ equal to 35.4° on pattern e indicates the presence of Fe_3O_4. A weak signal is also seen at 2θ equal to 43.4 suggesting the presence of the ε'-carbide phase, $Fe_{2.2}C$.

Pattern f was recorded for a sample which had been exposed to hydrogen and carbon monoxide for 56 days. Catalyst temperature was generally held between 200 and 240°C. The catalyst was exposed to 255°C for approximately 50 hr out of a total of 1340 hr of use. The broad peak centered at 2θ equal to 43.5° suggests the presence of several carbide phases. The peak is poorly resolved and particle size cannot be determined. Niemantsverdriet *et al.* (*10*) discuss the carbide phases generated under synthesis conditions. These can include ε'-, ε-, χ-,

TABLE 1

X-Ray Diffraction Data for Cu$K\alpha$

Phase	$2\theta^a$	T_c^b (°K)
α-Fe_2O_3	33.1	—
Fe_3O_4	35.4	—
α-Fe	44.5	—
ε'-$Fe_{2.2}C$	43.4	720
ε-Fe_2C	42.39	650
χ-Fe_5C_2	43.9	525
θ-Fe_3C	41.98	480

[a] Diffraction angle for the primary peak (*25*).

[b] Curie temperature.

and θ-carbide. The broad shape displayed by the used catalyst on Fig. 5 brackets the primary peaks for the first three. The used catalyst pattern has a shoulder at the location for α-Fe suggesting that α-Fe may also be present.

Induction is seen to convert α-Fe_2O_3/SiO_2 into a mixture of Fe_3O_4 and ε'-carbide. Exposure of the catalyst for a total of 56 days to reaction conditions converts the Fe_3O_4 and ε'-carbide into a mixture of carbides and possibly α-Fe. The bulk composition was not characterized following 1000 hr of exposure. Madon and Taylor (*12*) have suggested that the active surface may be different than the bulk phase. This is supported by the observations of Niemansverdriet *et al.* (*10*) who report detection of oxides at the surface of an iron carbide. The techniques employed in this study indicate a mixture of bulk phases are present, the surface composition is undetermined as is the particle size of the working catalyst.

Rate Measurement and Product Distributions

The surface area of the working catalyst was not determined in this study. Methanation rates are reported per gram of catalyst charged to the reactor. The rate was seen to increase with an increase in temperature and in the H_2/CO ratio.

Changes in the C_2 to C_6 product distribution as a function of synthesis variables are presented in Fig. 6 at a common WHSV of 22,274. Only normal alkanes and primary *n*-olefins are represented because they constitute the major species detected. Branched alkanes and internal olefins were detected at lower concentrations than the normal and primary compounds for C_4 and above.

The selectivity to higher hydrocarbons is seen to decrease with increasing temperature. An increase in the H_2/CO ratio at a constant temperature leads to a slight decrease in the selectivity to higher molecular weights. Both observations are consistent with the work of Madon and Taylor (*12*) at 10 atm.

The rate of CO_2 formation increases with increasing temperature and increasing H_2/CO ratio. A similar effect is seen for the rate of methane formation. However, the concentration of CO_2 decreases with increasing temperature and H_2/CO ratio. At all conditions investigated, the amount of CO_2 is less than the amount of CO converted into C_1 to C_6 normal products.

The trends in rate and concentration for CO_2 are consistent with the postulate that CO_2 is a secondary product (*12*) formed via the water–gas shift reaction

$$H_2O + CO \rightleftarrows CO_2 + H_2.$$

As the total synthesis rate increases the rate for water, the primary product, increases. If the water–gas shift reaction is at equilibrium (K_{eq} = 130 at 500°K), then an increase in water will lead to an increase in CO_2. An increase in temperature for the exothermic reaction shifts the equilibrium to the left. Increasing the H_2/CO ratio decreases the equilibrium concentration of CO_2. Shift activity has been reasoned to indicate the presence of magnetite, Fe_3O_4 (*12*).

A GC–MS chromatogram for the C_6 to C_{11} synthesis products is presented in Fig. 7. Straight chain α-olefins are the primary products. This was also true at the low weights, C_2 to C_5. A repeating pattern is seen for each carbon number. The branched alkanes elute first, followed by the α-olefin, normal alkane, and a mixture of branched and internal olefins.

The chromatogram shows a large peak centered at scan 2420 which is identified as toluene. The toluene is not an impurity introduced during sample collection, handling, or injection. The concentration of toluene relative to 1-heptene was observed to vary with synthesis conditions.

Other cyclic and aromatic products were observed. These include: cyclohexene, methylcyclohexene, benzene, styrene, xylenes, methylethylbenzenes, and diethylbenzenes. Additional cyclic products may have formed but were not observed in the

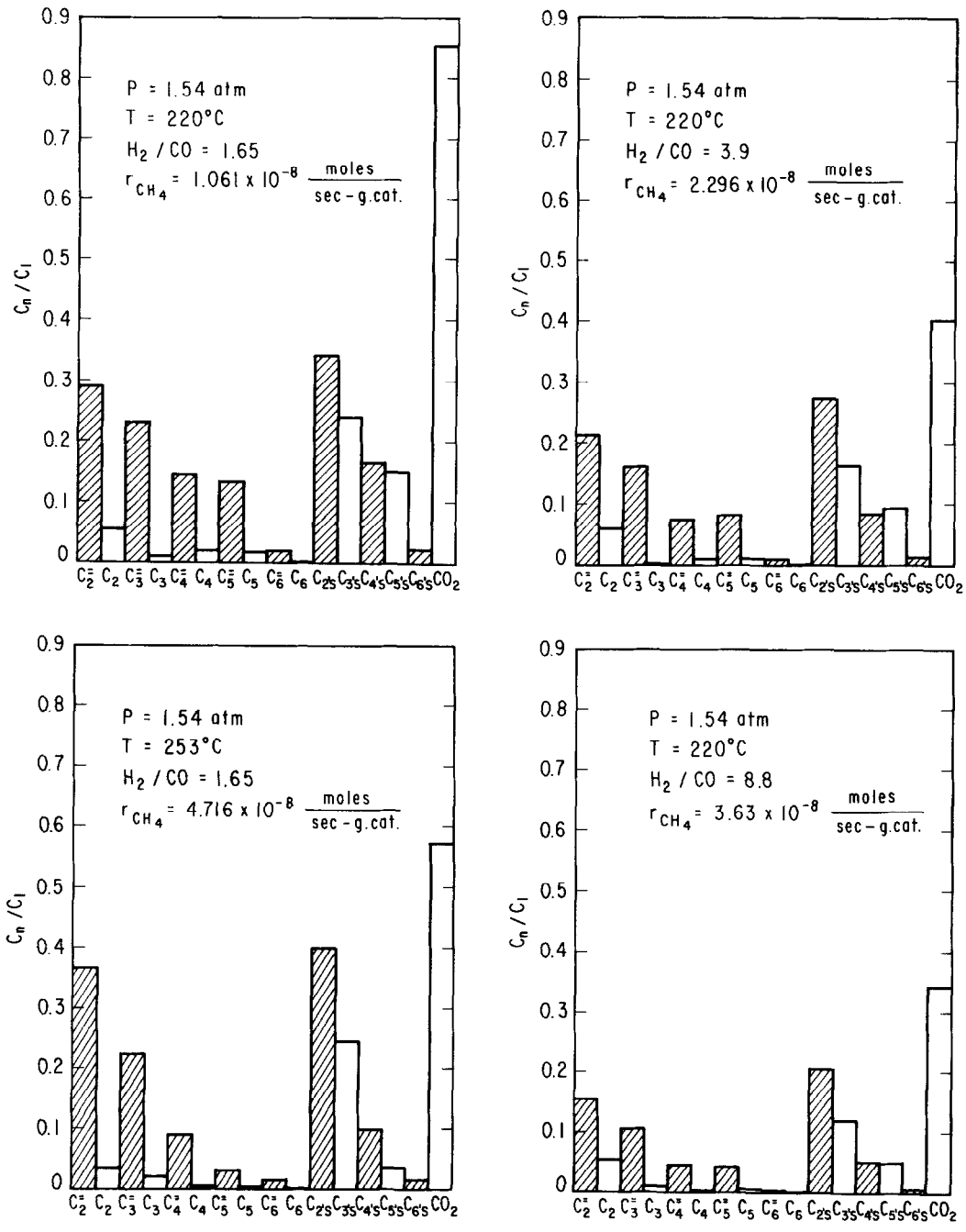

FIG. 6. Product distribution of the low weight synthesis products at WHSV of 22,274. Only *n*-alkanes and primary *n*-olefins are represented.

region of C_7 through C_{10}. Cyclic C_5 and C_6 alkanes and olefins as well as branched alkanes, olefins, and aromatics have been reported over unsupported iron-based catalysts (*16*). The effect of WHSV and synthesis conditions upon the distribution of cyclic hydrocarbons was not studied. Their presence was noted at different conditions; however, their concentration was not accurately determined.

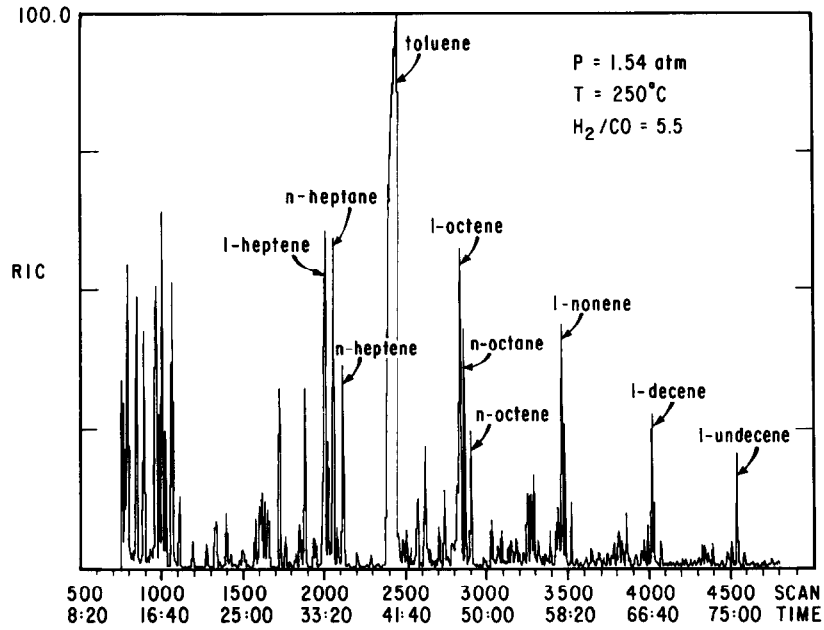

FIG. 7. Typical chromatogram of C_6 to C_{11} synthesis products at 250°C, 5.5/1 H_2/CO, 0.24 atm P_{CO}, 15,600 WHSV.

The presence of cyclic and aromatic compounds demonstrates that complex reactions are occurring during the hydrogenation of CO over Fe-based systems. Dwyer and Somorjai (*26*) report that olefins, the primary products, can readsorb and undergo incorporation into the regular Fischer–Tropsch products, acyclic hydrocarbons. They referred to this as secondary reaction. The means by which cyclic hydrocarbons and aromatics are formed are not revealed by this study. It seems reasonable to speculate that the primary and secondary products may readsorb and undergo surface rearrangements without incorporating into the growing chains.

Scavenging Experiments

The use of scavengers to chemically remove surface intermediates during Fischer–Tropsch synthesis is based upon the organometallic literature. Alkyl (*27*) and alkylidene ligands (*28–30*) of metal complexes are reported to undergo elimination reactions with olefins. The propagation reaction over Ru-based and Fe-based catalysts has been proposed (*18–20*) to involve methylene insertion into alkyl fragments. Chemical scavengers have been used over Ru-based catalysts (*21, 22*) and the results have been interpreted to support a methylene insertion process. This study was undertaken to determine if scavenging would work over Fe-based catalysts.

The ideal scavenger should react with surface hydrocarbon fragments and generate a product which is easy to detect and is not formed as a synthesis product. Cyclohexene was used over Ru (*21*) because Ru is known to synthesize acyclic products. Cyclohexene was alkylated by the elimination of alkyl or alkylidene ligands.

The present studies have shown that the synthesis product over iron is a complex mixture containing cyclohexene and methylcyclohexene. The feasibility of scavenging was tested by introducing a greater amount of cyclohexene into the reactant feed gas than was observed in the synthesis product stream.

Figure 8 shows a region of the GC chromatogram for the synthesis product and the

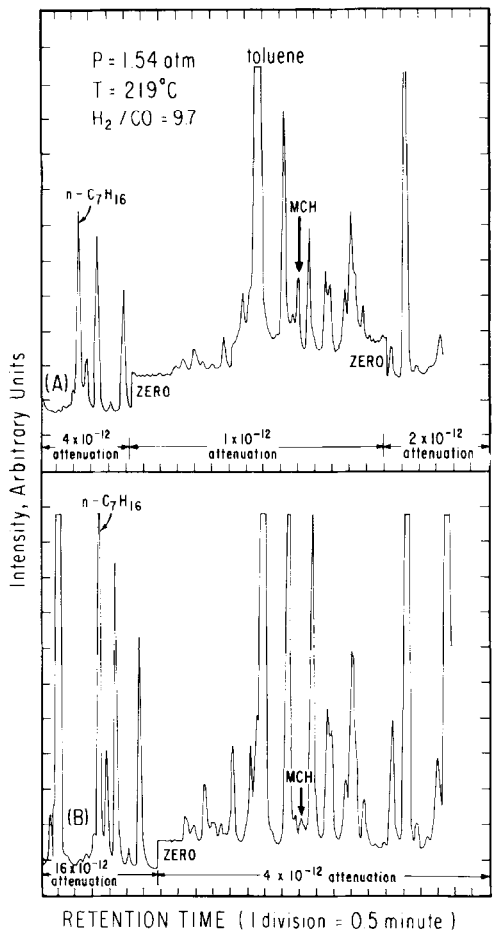

FIG. 8. Chromatogram in the presence of added cyclohexene (curve A) and under synthesis conditions (curve B) at 219°C, 9.7/1 H_2/CO, 0.14 atm CO, 14,590 WHSV.

cyclohexene scavenged product at 9.7 H_2/CO and 220°C. The CO conversion was approximately 0.8% at these conditions and a WHSV of 14,590. The location of methylcyclohexene is indicated on the figure. The assignment is made by comparison with GC–MS chromatograms, injection of pure compounds, and experience with the column elution characteristics. A slight increase in the methylcyclohexene signal is seen upon injecting cyclohexene 120 times. Methylcyclohexene/*n*-heptane is 0.012 and 0.083 for synthesis and scavenging, respectively.

Small amounts of methylcyclohexene, methycyclohexane, ethylcyclohexene, and ethylcyclohexane were formed upon addition of cyclohexene at H_2/CO ratios between 1.9 and 2.1 and temperatures between 220 and 255°C. The number of pulses and synthesis conditions were varied in an attempt to generate higher concentrations of alkyl-substituted cyclic compounds. In all cases the methyl-substituted compounds are present at a higher concentration than the ethyl-substituted compounds. These attempts were largely unsuccessful.

Pyridine was selected as a candidate scavenger because it contains a heteroatom, nitrogen, and low concentrations would be easy to discriminate from the multitude of synthesis products. The pyridine ring is difficult to hydrocrack between 200 and 250°C (*31*). Pyridine undergoes nucleophilic alkylation when treated with alkyllithium compounds (*32*). Finally, pyridine has been alkylated to 2-methylpyridine with $\frac{2}{1}$ H_2/CO over a Harshaw nickel catalyst, Ni-0104T, at 270°C (*33*).

Figure 9 presents a GC–MS chromatogram of the trapped products collected during the injection of 60 pulses of pyridine. The synthesis conditions were 1.65 H_2/CO at 250°C. The CO conversion was approximately 0.1% at these conditions and a WHSV of 22,275. Peaks for 2-methylpyridine and 2-ethylpyridine are indicated on the figure. Appropriate blank experiments were performed which established that the alkylpyridines are not impurities.

Additional experiments were performed at different synthesis conditions to confirm the generation of methyl- and ethylpyridines. Injections were reduced from 60 to between 3 and 10 in an attempt to minimize overloading the column with highly polar compounds. Tailing of pyridines was not eliminated, however, these studies indicated that three injections are sufficient to produce methyl- and ethylpyridine. The net effect of fewer injections is to increase the hydrocarbon signals on the chromatogram.

Only qualitative observations concerning the relative amount of C_1 and C_2 pyridines

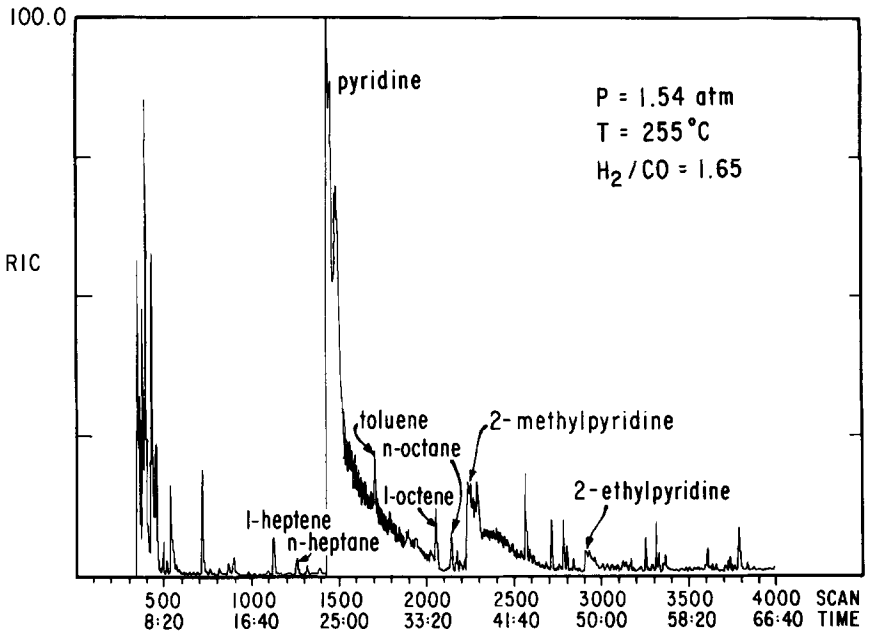

FIG. 9. Chromatogram in the presence of added pyridine at 255°C, 1.65/1 H_2/CO, 0.58 atm CO, 22,274 WHSV.

and changes in composition with synthesis conditions can be made using the OV-101 capillary column. Elution characteristics of polar compounds from a column designed for nonpolar compounds are such that peak areas can not be accurately assigned to the pyridines. The results show that the methylpyridine concentration is greater than the ethylpyridine concentration. One expects a higher concentration of methyl fragments on the surface during Fischer–Tropsch synthesis.

Additional studies (*34*) have been performed using a different capillary column, Carbowax on amine-deactivated fused silica. Propylpyridine is observed with this column. Relationships between the distribution of alkylpyridines and the synthesis conditions were found. These results and their implications with regard to the synthesis mechanism will be discussed in a future paper.

The mechanism by which pyridine is alkylated over the iron/silica catalyst is not known but can possibly be inferred from studies over nickel. Formation of 2-methylpyridine from H_2/CO (*33*) or alcohols (*33, 35*) over nickel was postulated to proceed via methyl addition to the α-carbon of pyridine, with pyridine bonded to the nickel surface through the nitrogen (*35*). Methyl groups were argued to form by interaction of H_2 and CO on the nickel surface. The source of CO being either direct addition with the reactant gas or indirect formation via alcohol decarbonylation. Methyl and higher alkyl fragments, which are expected over iron during Fischer–Tropsch synthesis, may interact with pyridine in a similar fashion to produce α-alkylpyridines.

A series of experiments were performed to establish whether the scavengers were reacting with hydrocarbon fragments on the metal phase or with reaction products which may have adsorbed on the silica support. A gas mixture consisting of 7.2% CO, 4944 ppm CH_4, and 500 ppm (nominal) each of CO_2, C_2H_4, C_2H_6, C_3H_6, C_3H_8, C_4H_8, C_4H_{10}, C_5H_{10}, C_5H_{12}, and C_6H_{14} was directed through the reactor. The reactor contained SiO_2 at 230°C and was operated at a WHSV of 16,000. Pulses of cyclohex-

ene or pyridine were injected into the gas mixture and the effluent was tested for alkyl-substituted scavengers. 2-Methylpyridine was observed at a ratio of 8.9×10^{-4} 2-methylpyridine/pyridine when pyridine was injected into the gas mixture. No alkylcyclohexenes or alkylcyclohexanes were detected.

The concentrations of C_1 to C_5 compounds in the gas mixture were a factor of 5 to 50 times greater than the Fischer–Tropsch products at 230°C. The ratio of methylpyridine/pyridine was a factor of 500 less than the ratio observed during scavenging studies under Fischer–Tropsch synthesis conditions. These observations suggest that the scavenger is removing hydrocarbon fragments from the metal phase, not products from the support phase, during scavenging under Fischer–Tropsch conditions.

Additional experiments were performed to determine if the scavengers were decomposing over the iron catalyst and if so whether the decomposition products were alkylating the scavengers. At 230°C and 16,000 WHSV of hydrogen pulses of pyridine were not found to decompose into C_1 to C_5 hydrocarbons. A trace amount of 2-methylpyridine was observed when pulses of pyridine were injected into hydrogen. The 2-methylpyridine was probably formed between pyridine and hydrogenated carbon residue. No other compounds, aside from pyridine, were detected.

Hydrogen was found to react with carbon present in or on the iron phase after the cessation of Fischer–Tropsch synthesis in a manner similar to that reported by Reymond *et al.* (*14*). Methane was observed as much as 24 hr after stopping the flow of CO. Methane was observed prior to injecting pyridine into the hydrogen stream.

Pulses of cylcohexene were also injected into 16,000 WHSV of hydrogen. The catalyst was maintained at 230°C under hydrogen for 24 hr prior to performing these experiments. Hydrogen alone led to methane. The methane signal increased by about 2 ppm and trace amounts, less than 1 ppm, of ethane and propane were observed when pulses of cyclohexene were added to the hydrogen. The slight increase in C_1–C_3 hydrocarbons suggests that the cyclohexene ring remains intact. A very weak signal was observed for methylcyclohexene when cyclohexene was injected into hydrogen. This is probably the result of cyclohexene interacting with hydrogenated carbon residue. Methylcyclohexene and C_1 to C_5 hydrocarbons were not observed when cyclohexene was added continuously to helium at a WHSV of 44 at 230°C.

Cyclohexene does interact over the catalyst. In the presence of helium or hydrogen, pulses of cyclohexene convert into a mixture of cyclohexene, cyclohexane, and benzene at 230°C. Since the C_1 to C_5 acyclic products are insignificant they can be eliminated as possible additional products. This assumption enables conversion of cyclohexene to be estimated. In the presence of helium, 0.22% of the cyclohexene reacted to cyclohexane, 0.48% reacted to benzene, and the balance remained unreacted. Hydrogen had a different effect. Twenty-nine percent of the cyclohexene reacted to cyclohexane and 15% reacted to benzene. The difference between hydrogen and helium was not studied. Both cyclohexene hydrogenation to cyclohexane and dehydrogenation to benzene are thermodynamically favored at 230°C, $K_{eq} = 4.8 \times 10^4$ and 300, respectively.

Pyridine and cyclohexene have different effects upon the C_2 to C_5 olefin to alkane ratio. Figure 10 presents the α-olefin to *n*-alkane ratio during Fischer–Tropsch synthesis and in the presence of a scavenger. The conversion of CO to C_1 to C_5 hydrocarbons are not reported because of the difficulty in actuating the GC's sample valve as the peak concentration of scavenged product passes through the sample loop. For this reason the ratios presented in Fig. 10 during scavenging should be taken as representative of the low weight products during scavenging and not taken as absolute. In

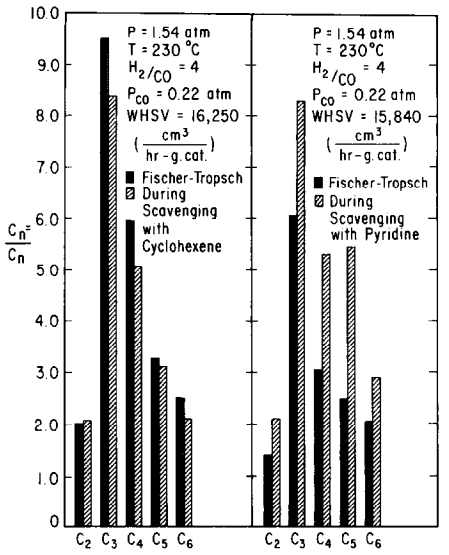

FIG. 10. Primary olefin to normal alkane selectivity in the presence and absence of scavenger at 230°C, ¼ H_2/CO, 0.22 atm CO.

general, the total conversion to CO was less in the presence of the scavenger.

The effect of pyridine and cyclohexene on the high weight products is shown in Figs. 11 and 12. Plots of log C_n/C_7 versus (n − 7) are presented for the Fischer–Tropsch products in the presence and absence of scavenger. The concentrations were determined using the four major components for a given carbon number, the normal alkane, the α-olefin, and two internal olefins. A basis of C_7 is chosen because this is the first carbon group which is well resolved on the capillary column.

Kellner and Bell (*36*) observed linear plots of log C_n/C_1 versus (n − 1) for Fischer–Tropsch synthesis over ruthenium. They incorporated this into a mechanistic and kinetic description of the synthesis reaction. The linear plot supports the methylene insertion mechanism in which alkyl fragments propagate to the next higher alkyl fragment by inserting CH_2 or terminate by hydrogenation to the alkane or by hydride elimination to the olefin. The slope of the line equals the log of the chain growth probability, α, where α = (propagation rate)/(propagation plus termination rates).

A plot of log C_n/C_7 versus (n − 7) has the same interpretation as log C_n/C_1 versus (n − 1) as long as the propagation and termination rate constants are independent of carbon number. The steeper the curve the lower the chain growth probability and the lower the average molecular weight of the product.

Straight lines are not observed for any condition reported in Figs. 11 and 12, and the Fischer–Tropsch lines are not identical for Figs. 11 and 12. The difference between Fischer–Tropsch curves and the nonlinear nature of the plots may be due to incomplete collection of the products in the liquid-nitrogen trap and to the fact that only four compounds for any given carbon number are used to determine concentration C_n. No attempt is made to interpret this nonlinear performance because of the uncertainty in the magnitude of C_n.

Figure 11 shows the average molecular weight of the C_7 to C_{16} hydrocarbon fraction decreases in the presence of cyclohexene. Three explanations can be given for the de-

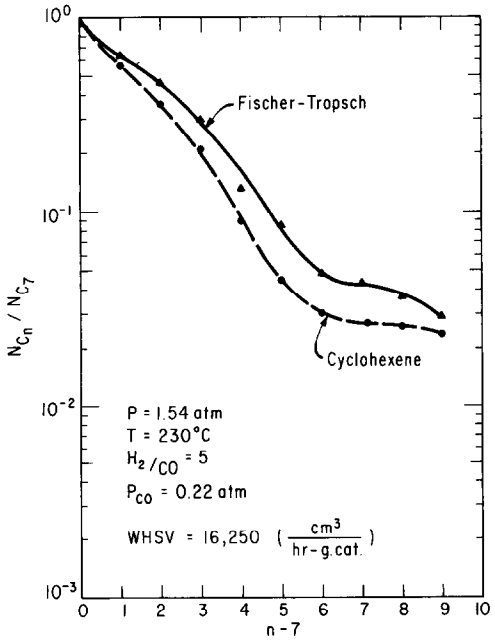

FIG. 11. Log(N_{C_n}/N_{C_7}) versus (n − 7) in the presence and absence of cyclohexene scavenger at 230°C, ¼ H_2/CO, 0.22 atm CO, 16,250 WHSV.

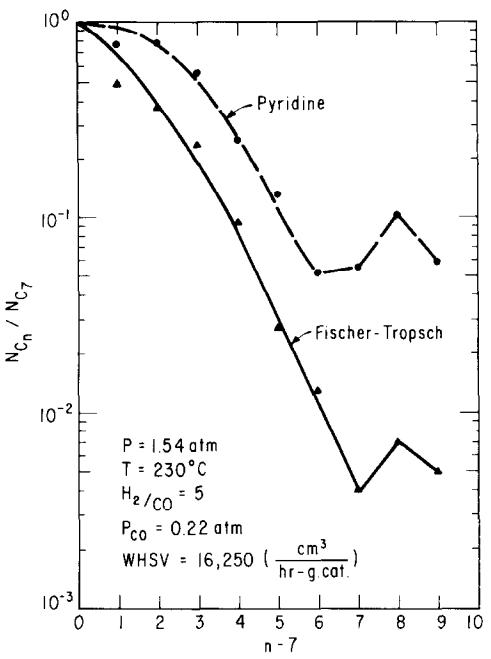

FIG. 12. Log(N_{C_n}/N_{C_7}) versus $n - 7$ in the presence and absence of pyridine scavenger at 230°C, $\frac{2}{1}$ H_2/CO, 0.22 atm CO, 16,250 WHSV.

crease in the chain length. Cyclohexene dehydrogenation to benzene is suggested by Fig. 10. This will act to increase the surface concentration of hydrogen and subsequently the rate of alkyl termination to alkanes. Cyclohexene may react with alkyl fragments to produce the alkylcyclohexenes observed upon injecting cyclohexene into the reaction mixture. This introduces a third alkyl fragment termination process. Both of these possibilities will act to increase the net rate of alkyl termination relative to propagation and thereby decrease the magnitude of α and the average molecular weight. The third possible explanation is removal of CH_2 groups in a manner similar to that reported over ruthenium (*21, 22*). This will reduce the concentration of CH_2 groups on the surface and simultaneously reduce the rate of propagation (*36*). A decrease in the rate of propagation will lead to a lower average molecular weight.

Figure 12 shows that the average molecular weight of the C_7 to C_{16} hydrocarbons increases in the presence of pyridine. The results shown in Fig. 10 suggest that pyridine displaces hydrogen from the surface. This may act to decrease the rate of termination of alkyl fragments to alkanes. Additional studies have shown that the distribution of alkylpyridines correlates with the Fischer–Tropsch product distribution, suggesting that pyridine is removing alkyl fragments from the catalyst surface (*34*). This removal may not be enough to compensate for the lower rate of termination by hydrogenation. The net effect of pyridine may be to reduce the total rate of alkyl termination and thereby increase the average molecular weight.

SUMMARY

The studies over 20 wt% Fe_2O_3/SiO_2 have shown that the iron phase converts into the same type of iron phases seen by other groups starting with Fe_3O_4 and Fe. The bulk phase is identified as a mixture of Fe_3O_4, carbides and possibly some α-Fe. The surface composition was not measured using surface sensitive spectroscopies. However, the conversion characteristics of CO_2 and the presence of aromatics suggest that some Fe_3O_4 is present at the surface of the carbides.

Synthesis products are analyzed through C_{16}. The primary products are the straight chain α-olefins. As the carbon number increases the complexity of the acyclic products increases to the level that branched alkanes constitute a larger fraction of synthesis products. Cyclohexene, methylcyclohexene, benzene, and alkyl-substituted benzenes were also observed as Fischer–Tropsch synthesis products. This suggests that even at low CO conversion in a differential reactor a complex set of reactions is present over iron.

Cyclohexene and pyridine were added to the reactant feed gas to scavenge hydrocarbon fragments from the surface. Both scavengers were alkylated, methyl sbustitution was greater than ethyl substitution. Pyridine was much more efficiently alkylated, 3

injections producing a measurable signal versus the 120 injections of cyclohexene required to see a minor increase in methylcyclohexene. Control experiments establish that the alkyl-substituted scavengers result from the interaction of the scavenger with hydrocarbon fragments formed with H_2 and CO on the iron phase. The fragments leading to α-alkylpyridines are probably alkyl fragments.

ACKNOWLEDGMENT

This work was supported by the Division of Chemical Sciences, Office of Basic Energy Sciences, U.S. Department of Energy, under Contract DE-AS05-80ER1072. The University of Texas Center for Energy Studies provided support for the gas chromatograph.

REFERENCES

1. Ott, G. L., Fleisch, T., and Delgass, W. N., *J. Catal.* **65,** 253 (1980).
2. Krebs, H. J., Bonzel, H. P., Schwarting, W., and Gafner, G., *J. Catal.* **72,** 199 (1981).
3. Dwyer, D. J., and Somorjai, G. A., *J. Catal.* **52,** 291 (1978).
4. Raup, G. B., and Delgass, W. N., *J. Catal.* **58,** 348 (1979).
5. Raup, G. B., and Delgass, W. N., *J. Catal.* **58,** 361 (1979).
6. Amelse, J. A., Butt, J. B., and Schwartz, L. H., *J. Phys. Chem.* **82,** 558 (1978).
7. Stanfield, R. M., and Delgass, W. N., *J. Catal.* **72,** 37 (1981).
8. Unmuth, E. G., Schwartz, L. H., and Butt, J. B., *J. Catal.* **63,** 404 (1980).
9. Amelse, J. A., Schwartz, L. H., and Butt, J. B., *J. Catal.* **72,** 95 (1981).
10. Niemantsverdriet, J. W., van der Kraan, A. M., van Dijk, W. L., and van der Baan, H. S., *J. Phys. Chem.* **84,** 3363 (1980).
11. King, D. L., *J. Catal.* **61,** 77 (1980).
12. Madon, R. J., and Taylor, W. F., *J. Catal.* **69,** 32 (1981).
13. Satterfield, C. N., and Huff, G. A., Jr., *J. Catal.* **73,** 187 (1982).
14. Reymond, J. P., Mériaudeau, P., and Teichner, S. J., *J. Catal.* **73,** 39 (1982).
15. Niemantsverdriet, J. W., and van der Kraan, A. M., *J. Catal.* **72,** 385 (1981).
16. Anderson, R. B., *in* "Catalysis" (P. H. Emmett, Ed.), Vol. 4. Reinhold, New York, 1956.
17. Biloen, P., and Sachtler, W. M. H., "Advances in Catalysis," Vol. 30, p. 163. Academic Press, New York 1981.
18. Bell, A. T., *Catal. Rev. Sci. Eng.* **23,** 203 (1981).
19. Brady, R. C., and Pettit, R., *J. Amer. Chem. Soc.* **103,** 1287 (1981).
20. Brady, R. C., and Pettit, R., *J. Amer. Chem. Soc.* **102,** 6181 (1980).
21. Ekerdt, J. G., and Bell, A. T., *J. Catal.* **62,** 19 (1980).
22. Bell, A. T., "Studies of the Mechanism and Kinetics of Fischer–Tropsch Synthesis over Ruthenium Catalysts," paper 9d, AIChE Annual Meeting, November, 1981.
23. Schultz, J. F., Hall, W. K., Seligman, B., and Anderson, R. B., *J. Amer. Chem. Soc.* **77,** 213 (1955).
24. Unmuth, E. E., Schwartz, L. H., and Butt, J. B., *J. Catal.* **61,** 242 (1980).
25. Berry, L. G., Ed., "Power Diffraction File, Inorganic Material." International Centre for Diffraction Data, Swarthmore, Pa., 1979.
26. Dwyer, D. J., and Somorjai, G. A., *J. Catal.* **56,** 249 (1979).
27. Evitt, E. R., and Bergman, R. G., *J. Amer. Chem. Soc.* **101,** 3973 (1979).
28. Fellman, J. D., Rupprecht, G. A., Wood, C. D., and Schrock, R. R., *J. Amer. Chem. Soc.* **100,** 5962 (1978).
29. Stevens, A. E., and Beauchamp, J. L., *J. Amer. Chem. Soc.* **100,** 2584 (1978).
30. Grubbs, R. H., and Miyashita, A., *J. Amer. Chem. Soc.* **100,** 7418 (1978).
31. Satterfield, C. N., and Cocchetto, J. F., *AIChE J.* **21,** 1107 (1975).
32. Abramovitch, R. A. (Ed.), "Pyridine and Its Derivatives," Vol. 14 Supplement, Part 2. Wiley, New York, 1974.
33. Myerly, R. C., and Weinberg, K. G., *J. Org. Chem.* **31,** 2008 (1966).
34. Wang, C. J., and Ekerdt, J. G., "Scavenging Alkyl Fragments with Pyridine during Fischer–Tropsch Synthesis Over Iron," Colloid and Surface Science Division paper 69, ACS National Meeting, Kansas City, 1982.
35. Reinecke, M. G., and Kray, L. R., *J. Amer. Chem. Soc.* **86,** 5355 (1964).
36. Kellner, C. S., and Bell, A. T., *J. Catal.* **70,** 418 (1981).